Bloch Chirality Induced by an Interlayer Dzyaloshinskii-Moriya Interaction in Ferromagnetic Multilayers

Shawn D. Pollard,[1] Joseph A. Garlow,[2,3] Kyoung-Whan Kim,[4] Shaobo Cheng,[3] Kaiming Cai,[1] Yimei Zhu,[2,3,*] and Hyunsoo Yang[1,†]

[1]Department of Electrical and Computer Engineering, National University of Singapore, Singapore 117576, Singapore
[2]Department of Materials Science and Chemical Engineering, Stony Brook University, Stony Brook, New York 11794, USA
[3]Condensed Matter Physics and Materials Science Division, Brookhaven National Laboratory, Upton, New York 11973, USA
[4]Center for Spintronics, Korea Institute of Science and Technology, Seoul, 02792, South Korea

(Received 6 February 2020; revised 11 September 2020; accepted 26 October 2020; published 23 November 2020)

Chiral spin textures stabilized by the interfacial Dzyaloshinkii-Moriya interaction, such as skyrmions and homochiral domain walls, have been shown to exhibit qualities that make them attractive for their incorporation in a variety of spintronic devices. However, for thicker multilayer films, mixed textures occur in which an achiral Bloch component coexists with a chiral Néel component of the domain wall to reduce the demagnetization field at the film surface. We show that an interlayer Dzyaloshinkii-Moriya interaction can break the degeneracy between Bloch chiralities. We further find large population asymmetries and chiral branching in the Bloch component of the domain walls in well-ordered Co/Pd multilayers. This asymmetry is a result of the combined effect of the demagnetization field and an interlayer Dzyaloshinkii-Moriya interaction, and is strongly related to film thickness and structural ordering. This work paves the way toward the utilization of this effect toward controlling Bloch chirality in magnetic multilayers.

DOI: 10.1103/PhysRevLett.125.227203

The antisymmetric exchange interaction, known as the Dzyaloshinskii-Moriya interaction (DMI), favors noncollinear, chiral alignment of spin textures and has garnered significant attention due to its role in the emergence of topological magnetic excitations such as magnetic skyrmions. These excitations have been proposed to play key roles in spintronic applications. In magnetic multilayers, this interaction is the result of symmetry breaking that occurs at interfaces between a magnetic layer and a heavy metal and lies in the plane of the interface, and, in the context of films with significant interlayer coupling, has been termed intralayer DMI. For ultrathin films and multilayers, significant intralayer DMI can result in homochiral Néel-type domain walls [1], or, for the proper balance of magnetic energies, the stabilization of Néel-type skyrmions [2–5].

However, key challenges remain toward their realization in devices. For example, in films with a greater magnetic volume, the spin texture can no longer be described by a single Néel chirality, but also contains an achiral Bloch component [6–8]. This complex domain profile may influence the dynamics of domains and domain walls in thicker magnetic films, such as by modulating the skyrmion Hall angle in films hosting skyrmions [6,9–11]. To control these effects, a means to break the degeneracy between Bloch domain orientations is necessary. However, it is expected that any Bloch component would be achiral due to the symmetry of standard micromagnetic energies [7,12,13].

Recently, it was demonstrated that DMI may lead to chiral coupling through interfaces wherein ferromagnetic layers are coupled through a heavy metal layer [14–16]. This interlayer DMI has been proposed as a mechanism for chiral hysteresis in synthetic antiferromagnets, and has been observed in Pt/CoFeB/Pt/Ru/Pt/Co/Pt, Pt/Co/Pt/Ru/Pt/Co/Pt, and Pt/CoSiB/Pt/CoSiB/Pt heterostructures [14,16]. The effect was suggested as a result of lateral symmetry breaking that occurs during sputter deposition processes, however, the precise microstructural origin is still unknown.

In this Letter, we report a clear chiral preference of Bloch-type domain walls in Co/Pd multilayers, which cannot be explained by the symmetry of solely the magnetic layers. We show a promising mechanism to break the degeneracy between the two possible chiralities of Bloch walls is interlayer DMI in the form of $D_{\text{inter}}\hat{\mathbf{z}} \cdot (\mathbf{m}_i \times \mathbf{m}_{i+1})$, which is the minimal model for the DMI satisfying bulk inversion asymmetry observed in our experiment where D_{inter} represents the interlayer DMI constant, $\mathbf{m}_i$ the magnetization in the ith layer of the film, and $\hat{\mathbf{z}}$ is orthogonal to the plane of the film [16]. Our experimental observations are consistent with the thickness dependencies predicted by our theory, supporting our claim. Our observations provide a physically interesting example that consideration of the *interlayer* chiral exchange coupling is essential for the chiral dependence of *intralayer* magnetic textures, which may be useful for further development of spintronics.

We first make a symmetry argument for the form of the interlayer DMI. We consider a general quadratic form of the DMI for a stack consisting of two-dimensional magnetic layers [14,17],

$$E_{\mathrm{DMI}} = \sum_i \int dx\, dy \left[\mathbf{D}_i^x \cdot (\mathbf{m}_i \times \partial_x \mathbf{m}_i) + \mathbf{D}_i^y \cdot (\mathbf{m}_i \times \partial_y \mathbf{m}_i) + \frac{1}{t+d} \mathbf{D}_i^z \cdot (\mathbf{m}_i \times \mathbf{m}_{i+1}) \right], \tag{1}$$

where i is the layer index along the z direction and $\mathbf{D}_i^{x,y,z}$ are the DMI vectors. While the DMI vectors can have angular dependencies due to crystal symmetry or higher order spin-orbit coupling [18], their effects are beyond quadratic interactions and are therefore neglected for the purpose of determining the primary interaction components. Chiral preference of the Bloch wall requires mirror symmetry breaking against all of the directions x, y, and z. Among the nine coefficients of the DMI, the symmetry breaking corresponds to the three coefficients $\mathbf{D}_i^u \cdot \hat{\mathbf{u}}$ for $u = x$, y, z [19–21]. For $u = x$, y, $\mathbf{D}_i^u \cdot \hat{\mathbf{u}}$ describes the intralayer DMI, which is inconsistent with our experimental observation regarding the dependence on the thickness and the number of layers and gives only small quantitative corrections (see Supplemental Material, 1 [22]). Dropping the two intralayer DMI terms, we conclude only the normal component $\mathbf{D}_i^z \cdot \hat{\mathbf{z}}$ is relevant for the chiral preference observed in our experiment. For simplicity, we ignore the spatial and layer dependence of $\mathbf{D}_i^z \cdot \hat{\mathbf{z}}$ for constructing a minimal model and denote $\mathbf{D}_i^z \cdot \hat{\mathbf{z}}/(t+d) = D_{\mathrm{inter}}$.

Now we illustrate how the normal component of the interlayer DMI can result in the Bloch-type chiral dependence of domain walls, when combined with the demagnetization field. For simplicity, we first consider a magnetic bilayer (denoted by the indices i and $i+1$), as shown schematically in Fig. 1(a). The domain wall tilting angles are ϕ_i and ϕ_{i+1}, respectively, and we take the angles in the range of $-\pi < \phi_i \leq \pi$. For thick structures, the magnetization of the domain boundary varies through the thickness of the structure to minimize the demagnetization energy [7,12,13,23,24], schematically shown in Fig. 1(b). This condition corresponds to $|\phi_2| > |\phi_1|$ in our situation, and their difference is determined by the relative magnitude of the demagnetization energy and the interlayer exchange coupling. Although this condition cannot determine any preference for the Bloch chirality (i.e., the sign of the tilting angles), the normal component of the interlayer DMI can break the degeneracy as follows. If D_{inter} is positive (negative), the interlayer DMI energy $D_{\mathrm{inter}}\hat{\mathbf{z}} \cdot (\mathbf{m}_1 \times \mathbf{m}_2)$ is minimized when $\phi_2 < \phi_1$ ($\phi_2 > \phi_1$), where $\hat{\mathbf{z}}$ is the thickness direction. The combination of the two conditions above determines the sign of the tilting angles to be negative (positive). This argument is demonstrated in Fig. 1(b) and shows that the combined effect of the demagnetization field and the interlayer DMI, together, may break the symmetry of the two Bloch chiralities.

The above argument may be generalized to a multilayer structure consisting of N magnetic layers with thickness t, separated by $N-1$ normal metal layers with thickness d, with each magnetic layer denoted by the index i. We consider a minimal model consisting of three energy terms for interlayer coupling: the interlayer exchange coupling $E_{\mathrm{exc}} = -J_{\mathrm{inter}} \int dx\, dy \sum_i \mathbf{m}_i \cdot \mathbf{m}_{i+1}$, the interlayer DMI $E_{\mathrm{DMI}} = D_{\mathrm{inter}} \int dx\, dy \sum_i \hat{\mathbf{z}} \cdot (\mathbf{m}_i \times \mathbf{m}_{i+1})$, and the interlayer demagnetization energy $E_{\mathrm{demag}} = -(\mu_0 M_s^2/4\pi) \sum_{i<j} \int d\mathbf{r}_i\, d\mathbf{r}_j [3(\mathbf{m}_i \cdot \hat{\mathbf{r}}_{ji})(\mathbf{m}_j \cdot \hat{\mathbf{r}}_{ji}) - \mathbf{m}_i \cdot \mathbf{m}_j]/|\mathbf{r}_i - \mathbf{r}_j|^3$, where μ_0 is the magnetic permeability, M_s is the saturation magnetization, and $\hat{\mathbf{r}}_{ji}$ is the unit vector along $\mathbf{r}_j - \mathbf{r}_i$. Intralayer contributions are considered by adopting the domain wall profile $\mathbf{m}_i(x_i) = (\cos\phi_i \mathrm{sech} x_i/\lambda, \sin\phi_i \mathrm{sech} x_i/\lambda, \tanh x_i/\lambda)$, where λ is the domain wall width, and the total energy is written as a function of the tilting angles $E_{\mathrm{total}}(\{\phi_i\}) = E_{\mathrm{exc}} + E_{\mathrm{DMI}} + E_{\mathrm{demag}}$. The energy minimizing set of tilting angles $\{\phi_i\}$ determines the chirality of the domain walls.

The energy difference between the two Bloch chiralities, up to first order in $1/J_{\mathrm{inter}}$, following the derivation in Supplemental Material, 1 [22], is given by

$$\begin{aligned} \Delta E_{\mathrm{chiral}} &= E_{\mathrm{total}}(\bar{m}_y > 0) - E_{\mathrm{total}}(\bar{m}_y < 0) \\ &= \frac{D_{\mathrm{inter}}}{J_{\mathrm{inter}}} f(d, t, N), \end{aligned} \tag{2}$$

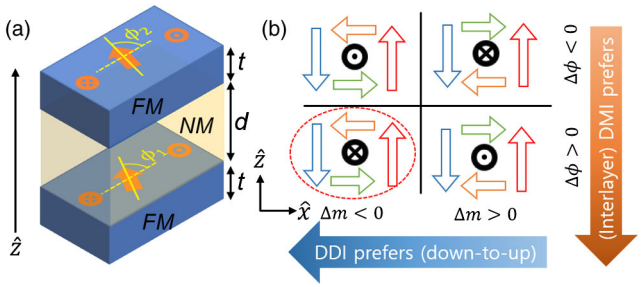

FIG. 1. (a) Schematic of a typical multilayer geometry used to model the effects of interlayer DMI, consisting of two ferromagnetic layers (FM) of thickness t and a nonmagnetic spacer (NM) of thickness d. (b) Schematic diagram of a domain wall spin structure demonstrating the influence of interlayer DMI and dipole-dipole interactions (DDI), which results in a preferential rotation of the magnetization through the multilayer thickness and a Bloch chirality. The DDI preferentially favors a flux closure state, selecting the initial magnetization orientation at both surfaces, while interlayer DMI preferentially favors one direction of rotation between the surfaces. Here, $\Delta\phi = \phi_2 - \phi_1$ and $\Delta m_x = m_{x,2} - m_{x,1}$. Note that $|\phi_2| > |\phi_1|$ in the text is equivalent to $\Delta m_x < 0$ in the figure. The schematic shown here assumes a negative interlayer DMI, while $\odot$ and $\otimes$ denote the average domain wall magnetization lying along the $-y$ and $+y$ directions, respectively.

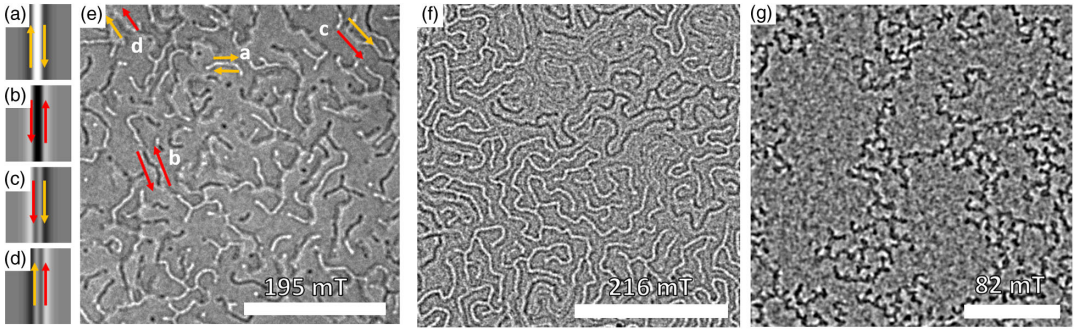

FIG. 2. (a)–(d) Numerically calculated LTEM contrast for the domain wall orientation across a 360° domain indicated by the red (CCW) and orange (CW) arrows. (e) Domain contrast for the $[\mathrm{Co}\,7\,\mathrm{Pd}\,5]_{15}$ sample taken with a 195 mT field along the microscope axis. No obvious asymmetry from bright and dark domains is present. Regions corresponding to simulated images in (a)–(d) are indicated. (f) Domain contrast for the $[\mathrm{Co}\,7\,\mathrm{Pd}\,5]_{30}$ sample taken at 216 mT, with a large asymmetry between bright and dark domains, indicative of a symmetry breaking interaction favoring CW Bloch walls. (g) A difference image obtained by subtracting underfocus and overfocus images for the $[\mathrm{Co}\,9\,\mathrm{Pd}\,10]_{30}$ sample, taken at 82 mT. A lowpass filter has been applied to reduce high frequency noise. The image has been inverted for clarity. No CCW domains are apparent, which would appear as bright regions in the inverted image. The scale bars represent 2 μm.

where $\bar{m}_y$ is the averaged m_y at the domain wall center over the N magnetic layers, with $f(d,t,N)$ presented in Supplemental Material, 1 [22]. We note that $f(d,t,N)$ is proportional to the demagnetization energy, and thus the chirality-dependent energy $\Delta E_{\mathrm{chiral}}$ is a consequence of the demagnetization energy and the interlayer DMI. From Eq. (2), the energetically preferred chirality is determined by the sign of D_{inter}, thereby offering a potential avenue in which to design systems with Bloch chirality in nominally centrosymmetric multilayers. Evaluating $\Delta E_{\mathrm{chiral}}$ for different repetition numbers, magnetic and nonmagnetic thicknesses demonstrates that increasing the ferromagnetic layer volume, and hence demagnetization energies, affords a straightforward means to increase the energy difference between chiralities, while decreasing the nonmagnetic layer thickness similarly results in an increase in the energy difference, as detailed in Supplemental Material, 2 and Supplemental Material, Fig. 1 [22].

The theoretical model described above was found to be consistent with observations of domain asymmetries in Co/Pd multilayers of the form substrate/MgO(2 nm)/Pt(4 nm)/Co(X)/[Pd(Y)/Co(X)]$_z$/Pt(4 nm), where X and Y are the Co and Pd thickness, in angstroms, respectively, and z is the multilayer repetition, which were grown by magnetron sputtering on thermally oxidized Si substrates for structural and bulk magnetometry characterization, as shown in the Supplemental Material, Figs. 2 and 3 [22], and on Si_3N_4 membranes for Lorentz transmission electron microscopy (LTEM) measurements of the magnetic structure. Co/Pd is a well-studied system in which the magnetic properties can be modified by tuning the thicknesses of the constituent layers [25–28]. We utilize a labeling convention of $[\mathrm{Co}X\mathrm{Pd}Y]_z$ for all films mentioned in the text.

With LTEM, contrast formation is classically explained by the deflection of the electron beam when it passes through a magnetic field, which results in either enhanced or decreased intensity at regions of nonuniform magnetization. For a system with perpendicular magnetic anisotropy at zero sample tilt, the resulting contrast is proportional to the Bloch component of the magnetization at a domain boundary. Figures 2(a)–2(d) show calculated LTEM image contrast for possible domain wall structures taken underfocus and within the small defocus limit [24,29]. Clockwise (CW) Bloch domain walls, wherein the Bloch component of the magnetization rotates clockwise between opposing sides of a 360° domain, exhibit alternating dark-bright contrast, while counterclockwise (CCW) Bloch walls with an opposite sense of rotation will exhibit bright-dark contrast [30,31]. For 360° domains with a consistent sense of rotation, the central domain contrast will be enhanced due to the overlap of contrast from domain wall edges. For mixed 360° domain walls (i.e., CW rotation from $-z$ to $+z$ and CCW from $+z$ to $-z$ or vice versa), the net contrast will decrease.

Figures 2(e)–2(g) show typical magnetization states after saturation and relaxation to the indicated field values for the $[\mathrm{Co}\,7\,\mathrm{Pd}\,5]_{15}$, $[\mathrm{Co}\,7\,\mathrm{Pd}\,5]_{30}$, and $[\mathrm{Co}\,9\,\mathrm{Pd}\,10]_{30}$ samples, respectively. For $[\mathrm{Co}\,7\,\mathrm{Pd}\,5]_{15}$ with a magnetic thickness of 18.7 nm, no obvious asymmetry in CW and CCW domain populations is observed. However, a clear population asymmetry is observed in $[\mathrm{Co}\,7\,\mathrm{Pd}\,5]_{30}$ with a magnetic thickness of 36.7 nm. To approximate this asymmetry, we divided 20 distinct images into grids of 2000 nm^2 cells, and then assigned each cell value of 1 or 0 for each grid point containing a CW domain. A similar method was done for CCW domains. The probability of CW domains, $P(\mathrm{CW})$, was taken to be

$$P(\mathrm{CW}) = \frac{N(\mathrm{CW})}{N(\mathrm{CW}) + N(\mathrm{CCW})},$$

where $N(\mathrm{CW})$ and $N(\mathrm{CCW})$ are the number of cells containing CW and CCW domains, respectively. Additional images are shown in Supplemental Material, Fig. 4 [22]. No significant variation is observed as a function of applied field (Supplemental Material, Fig. 5 [22]). This lack of variation is expected as the out-of-plane field does not significantly alter the internal domain wall structure following nucleation. Averaged over all fields, $P(\mathrm{CW})$ was measured as 0.79 ± 0.10. The uncertainty is estimated as the standard deviation of $P(\mathrm{CW})$ obtained from each individual image. Using the same method, this compares to the weak asymmetry of $P(\mathrm{CW}) = 0.56 \pm 0.03$ for $[\mathrm{Co\,7\,Pd\,5}]_{15}$. This change in asymmetry with repetition number is in qualitative agreement with the numerical results for interlayer DMI shown in Supplemental Material, Fig. 1(a) [22].

For $[\mathrm{Co\,9\,Pd\,10}]_{30}$ [Fig. 2(g)], only CW domains were observed, albeit with weaker contrast due to the increased nonmagnetic Pd thickness. Complete domain asymmetries were also observed in a $[\mathrm{Co\,8\,Pd\,15}]_{30}$ sample (see Supplemental Material, Fig. 6 [22]). An additional $[\mathrm{Co\,9\,Pd\,15}]_{30}$ was imaged. While no CCW domains were observed, the weak contrast prevents conclusive claims of a 100% asymmetry in the $[\mathrm{Co\,9\,Pd\,15}]_{30}$ sample (see Supplemental Material, Fig. 7 [22]). The increase in domain asymmetries observed for $[\mathrm{Co\,9\,Pd\,10}]_{30}$ is expected due to the different energy scaling for changes in magnetic and nonmagnetic layer thicknesses, as shown in Supplemental Material, Figs. 1(b) and 1(c) [22].

We further explore the role of an in-plane magnetic field during relaxation of the magnetization from out-of-plane saturation. As an out-of-plane magnetic field is relaxed at tilt, 360° domains will nucleate and propagate nominally along the in-plane magnetic field direction, as shown in Supplemental Material, Fig. 8 [22]. Because of the in-plane field, both boundaries of the 360° domain wall will align along the in-plane field, i.e., one wall CW, the other CCW, depending on the relative orientation of the field. During the relaxation process, the domain may also expand via branching [32,33], where branches will be either CW or CCW, as shown schematically in Fig. 3(a). If there is a difference in energy density along CW and CCW domain walls, branching will occur preferentially from one side of the domain boundary. We term this chiral branching.

From our previous experiments, we expect chiral branching in the $[\mathrm{Co\,7\,Pd\,5}]_{30}$ sample, with larger populations of CW branches. Clear population asymmetries are indeed observed, as shown in Figs. 3(b)–3(g) and in Supplemental Material, Fig. 9 [22]. We found a net total of 1253 events with a CW branching probability of 73.9% over a series of images. Assuming each branching can occur with a 50% probability, the asymmetry is ~17 standard deviations from the expected value. Contrary to initial expectations, a larger degree of chiral branching, approximately 64.9% with an

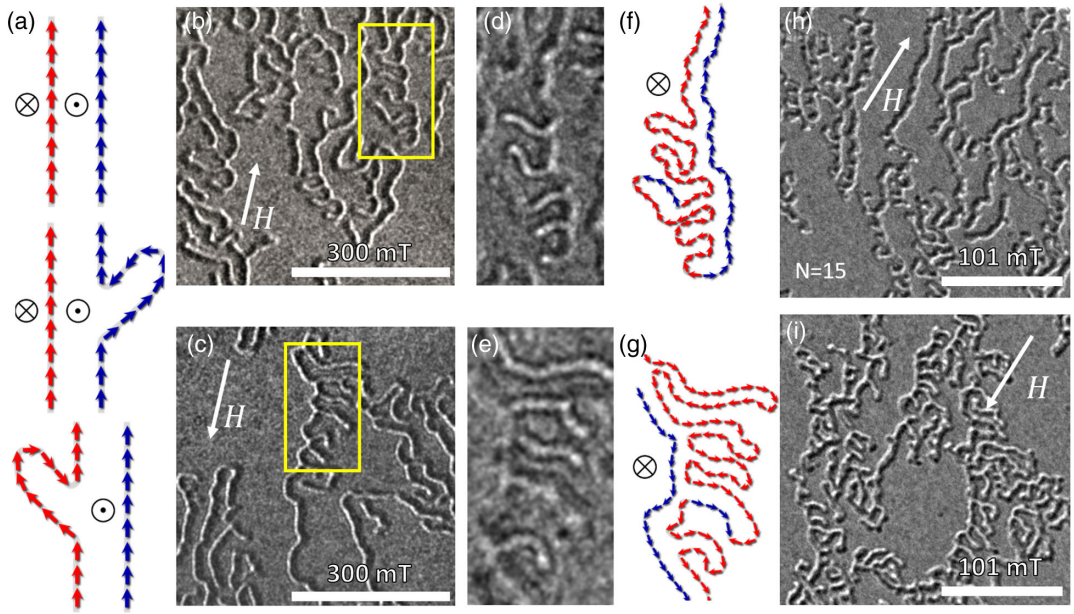

FIG. 3. Domain propagation behavior under the influence of an in-plane applied field. (a) Schematic of the approximate domain wall structure during the branching process, showing both possible CW (red) and CCW (blue) branching directions. (b),(c) Representative measurements of chiral branching taken at (b) 30 and (c) −30° tilts at 300 mT for the $[\mathrm{Co\,7\,Pd\,5}]_{30}$ sample. The white arrow indicates the in-plane field direction. The selected areas marked by the yellow box correspond to the region shown in (d),(e), respectively. Bright (dark) regions indicate CW (CCW) branching, with the approximate domain wall spin structure of a selected branching structure shown in (f) and (g) for clarity, with red (blue) regions indicating CW (CCW) domain boundaries. (h),(i) Same as (b),(c), but for the $[\mathrm{Co\,7\,Pd\,5}]_{15}$ sample, taken at 101 mT, exhibiting chiral branching, as evidenced by the extensive branching along the left (h) and right (i) sides of the main domains. All scale bars are 2 μm.

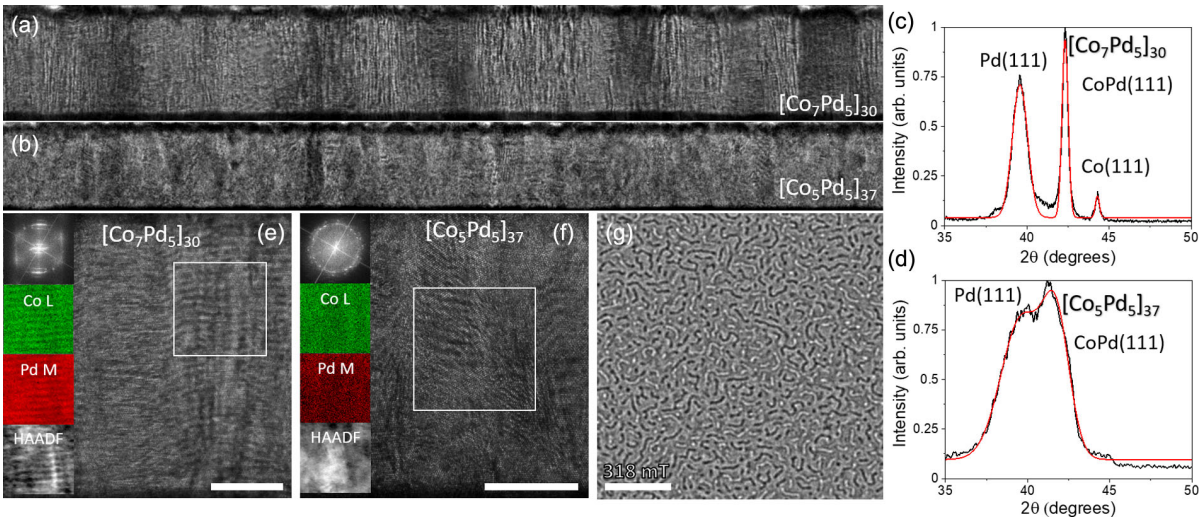

FIG. 4. (a) and (b) show low magnification HRTEM images of the $[\mathrm{Co}\,7\,\mathrm{Pd}\,5]_{30}$ and $[\mathrm{Co}\,5\,\mathrm{Pd}\,5]_{37}$ multilayers to compare their granular morphology. The image widths are 370 nm. (c) and (d) show XRD measurements corresponding to the same samples. Red lines are fits. (e) and (f) show HR-TEM images corresponding to both samples, respectively. The upper insets depicting the fast Fourier transform of the images show the ordered texturing present in the $[\mathrm{Co}\,7\,\mathrm{Pd}\,5]_{30}$ sample and not in the $[\mathrm{Co}\,5\,\mathrm{Pd}\,5]_{37}$ sample, as confirmed by annular dark field imaging and EELS mapping of the Co L edge and Pd M edge. The scale bars represent 10 nm. (g) Magnetic domain configuration of the $[\mathrm{Co}\,5\,\mathrm{Pd}\,5]_{37}$ multilayer taken with a field of 318 mT with no notable domain asymmetries. The scale bar represents 2 μm.

asymmetry ~6 standard deviations from the random case, was also observed in the $[\mathrm{Co}\,7\,\mathrm{Pd}\,5]_{15}$ sample, as shown in Figs. 3(h) and 3(i), in contrast to the much smaller asymmetry observed with the field applied perpendicular to the film plane. This may be a result of the influence of the external field on the domain wall structure, which results in a broadening of the domain wall in the plane of the film [34], and a corresponding increase $\Delta E_{\mathrm{chiral}}$, as well as a straightening of the domain wall through the film thickness [35], which would lead to a decrease in $\Delta E_{\mathrm{chiral}}$. While the influence of these two effects is of opposite sign, they do not necessarily cancel. A thinner $[\mathrm{Co}\,7\,\mathrm{Pd}\,5]_{10}$ sample with a smaller magnetic thickness showed no indication of branching asymmetries at tilt, as shown in Supplemental Material, Fig. 10.

We further studied the role of structural ordering on Bloch asymmetries, which has been suggested to play a key role in the presence of interlayer DMI [14–16]. We prepared a $[\mathrm{Co}\,5\,\mathrm{Pd}\,5]_{37}$ sample with nominally identical Co/Pd volume as $[\mathrm{Co}\,7\,\mathrm{Pd}\,5]_{30}$, as shown in Figs. 4(a) and 4(b). Figures 4(c) and 4(d) show XRD measurements of the two samples, where clear, narrow peaks corresponding to FCC(111) textured Co, Pd, and CoPd alloy are observed only for the $[\mathrm{Co}\,7\,\mathrm{Pd}\,5]_{30}$ sample. Figures 4(e) and 4(f) show high resolution (HR) TEM and corresponding fast Fourier transform for both samples, as well as electron energy loss spectrum (EELS) maps. For $[\mathrm{Co}\,7\,\mathrm{Pd}\,5]_{30}$, with clear population asymmetries, superlattice peaks, and compositional modulation were observed. However, for the $[\mathrm{Co}\,5\,\mathrm{Pd}\,5]_{37}$ sample, no evidence of similar ordering was seen, indicating that 0.5 nm Co is too thin to establish a strongly ordered multilayer. As shown in Fig. 4(g), no domain asymmetry was observed in the $[\mathrm{Co}\,5\,\mathrm{Pd}\,5]_{37}$ sample $[P(\mathrm{CW}) = 0.48 \pm 0.08]$, in line with expectations. We note that while the total Co/Pd volume is similar between samples, the total magnetic moment is approximately 19% weaker for $[\mathrm{Co}\,5\,\mathrm{Pd}\,5]_{37}$ due to a lower net Co thickness, as determined by vibrating sample magnetometry shown in Supplemental Material, Figs. 2 and 3. While this could result in a reduced asymmetry, it is still expected to be greater than that of $[\mathrm{Co}\,7\,\mathrm{Pd}\,5]_{15}$, and therefore we conclude the lack of domain asymmetries is likely due to a lack of clear multilayer ordering. Large Bloch asymmetries were also observed in qualitatively similar Ir/Fe/Gd/Fe/Pt multilayers using LTEM [24], without asymmetries in Fe/Gd multilayers lacking heavy metal layers, indicating this phenomena may be applicable to a large class of multilayer systems.

One candidate of the microscopic origin of the interlayer DMI is nontrivial formation of the interface between the Pd and Co layer, breaking mirror symmetry in all three directions. Then spin-orbit coupling of the form $\sigma_z p_z$ is allowed for electrons near the interface and the RKKY interaction mediated by the spin-orbit coupled electrons leads to the z component of the interlayer DMI. The different formation of Co/Pd and Pd/Co interfaces during the sputtering process will result in a net interlayer DMI, similar to that proposed by Han *et al.* [14]. This difference is known to be universal as observed for nominally symmetric stacks such as Pt/Co/Pt and Pd/Co/Pd. However, we defer more extensive and clearer understanding to future works.

In conclusion, we demonstrated large asymmetries in domain wall populations in Co/Pd multilayers, in line with predictions for an interlayer DMI. These asymmetries show a thickness and repetition dependence in agreement with our numerical models of an interlayer DMI, and a dependence on structural ordering consistent with recent reports of an interlayer DMI. These results cannot be explained by conventional micromagnetic theory or an intralayer DMI. This work suggests a new phenomenon associated with interlayer DMI and opens the possibility for controlling Bloch chirality in sputtered systems with centrosymmetric constituent elements. Through proper tuning of both interlayer and intralayer effects, this work provides a pathway toward the design of magnetic devices that avoid unwanted effects such as the skyrmion Hall effect, in line with the method proposed in Ref. [6].

We thank Kim Kisslinger for assistance in TEM sample preparation. This research was supported by SpOT-LITE program (A*STAR Grant No. A18A6b0057) through RIE2020 funds, the U.S. Department of Energy, Office of Basic Energy Sciences, Division of Materials Science and Engineering, under Contract No. DE-SC0012704. Research carried out, in part, at the Center for Functional Nanomaterials, Brookhaven National Laboratory, which is supported by the U.S. Department of Energy, Office of Basic Energy Sciences, under Contract No. DE-AC02-98CH10886. K.-W. K. acknowledges the support from the KIST Institutional program (2E30600), the National Research Council of Science & Technology (NST) (CAP-16-01-KIST), and the National Research Foundation (NRF) of Korea (2019M3F3A1A02071509, 2020R1C1C1012664).

J. A. G. and S. D. P. contributed equally to this work.

*zhu@bnl.gov
†eleyang@nus.edu.sg

[1] M. J. Benitez, A. Hrabec, A. P. Mihai, T. A. Moore, G. Burnell, D. Mcgrouther, C. H. Marrows, and S. McVitie, Nat. Commun. **6**, 8957 (2015).
[2] S. D. Pollard, J. A. Garlow, J. Yu, Z. Wang, Y. Zhu, and H. Yang, Nat. Commun. **8**, 14761 (2017).
[3] S. Woo, K. Litzius, B. Krüger, M.-Y. Im, L. Caretta, K. Richter, M. Mann, A. Krone, R. M. Reeve, M. Weigand, P. Agrawal, I. Lemesh, M.-A. Mawass, P. Fischer, M. Kläui, and G. S. D. Beach, Nat. Mater. **15**, 501 (2016).
[4] O. Boulle, J. Vogel, H. Yang, S. Pizzini, D. de Souza Chaves, A. Locatelli, T. O. Menteş, A. Sala, L. D. Buda-Prejbeanu, O. Klein, M. Belmeguenai, Y. Roussigné, A. Stashkevich, S. M. Chérif, L. Aballe, M. Foerster, M. Chshiev, S. Auffret, I. M. Miron, and G. Gaudin, Nat. Nanotechnol. **11**, 449 (2016).
[5] A. Soumyanarayanan, M. Raju, A. L. G. Oyarce, A. K. C. Tan, M.-Y. Im, A. P. Petrović, P. Ho, K. H. Khoo, M. Tran, C. K. Gan, F. Ernult, and C. Panagopoulos, Nat. Mater. **16**, 898 (2017).
[6] K.-W. Kim, K.-W. Moon, N. Kerber, J. Nothhelfer, and K. Everschor-Sitte, Phys. Rev. B **97**, 224427 (2018).
[7] W. Legrand, J.-Y. Chauleau, D. Maccariello, N. Reyren, S. Collin, K. Bouzehouane, N. Jaouen, V. Cros, and A. Fert, Sci. Adv. **4**, eaat0415 (2018).
[8] Y. Dovzhenko, F. Casola, S. Schlotter, T. X. Zhou, F. Büttner, R. L. Walsworth, G. S. D. Beach, and A. Yacoby, Nat. Commun. **9**, 2712 (2018).
[9] K. Litzius, I. Lemesh, B. Krüger, P. Bassirian, L. Caretta, K. Richter, F. Büttner, K. Sato, O. A. Tretiakov, J. Förster, R. M. Reeve, M. Weigand, I. Bykova, H. Stoll, G. Schütz, G. S. D. Beach, and M. Kläui, Nat. Phys. **13**, 170 (2017).
[10] S. Woo, K. M. Song, X. Zhang, Y. Zhou, M. Ezawa, S. Finizio, J. Raabe, J. W. Choi, B.-C. Min, H. C. Koo, and J. Chang, Nat. Commun. **9**, 959 (2018).
[11] W. Jiang, X. Zhang, G. Yu, W. Zhang, M. B. Jungfleisch, J. E. Pearson, O. Heinonen, K. L. Wang, Y. Zhou, A. Hoffmann, and S. G. E. te Velthuis, Nat. Phys. **13**, 162 (2017).
[12] J.-Y. Chauleau, W. Legrand, N. Reyren, D. Maccariello, S. Collin, H. Popescu, K. Bouzehouane, V. Cros, N. Jaouen, and A. Fert, Phys. Rev. Lett. **120**, 037202 (2018).
[13] J. A. Garlow, S. D. Pollard, M. Beleggia, T. Dutta, H. Yang, and Y. Zhu, Phys. Rev. Lett. **122**, 237201 (2019).
[14] D.-S. Han, K. Lee, J.-P. Hanke, Y. Mokrousov, K.-W. Kim, W. Yoo, Y. L. W. van Hees, T.-W. Kim, R. Lavrijsen, C.-Y. You, H. J. M. Swagten, M.-H. Jung, and M. Kläui, Nat. Mater. **18**, 703 (2019).
[15] E. Y. Vedmedenko, P. Riego, J. A. Arregi, and A. Berger, Phys. Rev. Lett. **122**, 257202 (2019).
[16] A. Fernández-Pacheco, E. Vedmedenko, F. Ummelen, R. Mansell, D. Petit, and R. P. Cowburn, Nat. Mater. **18**, 679 (2019).
[17] K. M. D. Hals and K. Everschor-Sitte, Phys. Rev. Lett. **119**, 127203 (2017).
[18] I. A. Ado, A. Qaiumzadeh, A. Brataas, and M. Titov, Phys. Rev. B **101**, 161403(R) (2020).
[19] K. V. Samokhin, Ann. Phys. (Amsterdam) **324**, 2385 (2009).
[20] S. J. Lee, K. W. Kim, H. W. Lee, and K. J. Lee, J. Magn. Magn. Mater. **455**, 14 (2018).
[21] S. Mühlbauer, B. Binz, F. Jonietz, C. Pfleiderer, A. Rosch, A. Neubauer, R. Georgii, and P. Böni, Science **323**, 915 (2009).
[22] See Supplemental Material at http://link.aps.org/supplemental/10.1103/PhysRevLett.125.227203 for a derivation of Eq. (2), as well as magnetometry measurements and additional images of chiral asymmetries in multilayers shown in the text.
[23] S. A. Montoya, S. Couture, J. J. Chess, J. C. T. Lee, N. Kent, D. Henze, S. K. Sinha, M.-Y. Im, S. D. Kevan, P. Fischer, B. J. McMorran, V. Lomakin, S. Roy, and E. E. Fullerton, Phys. Rev. B **95**, 024415 (2017).
[24] J. J. Chess, S. A. Montoya, E. E. Fullerton, and B. J. McMorran, AIP Adv. **7**, 056807 (2017).
[25] V. Kamberský, P. de Haan, J. Šimšová, S. Porthun, R. Gemperle, and J. C. Lodder, J. Magn. Magn. Mater. **157–158**, 301 (1996).
[26] F. Hakkens, A. De Veirman, W. Coene, and B. F. J. A. den, J. Mater. Res. **8**, 1019 (1993).

[27] S. Hashimoto, Y. Ochiai, and K. Aso, J. Appl. Phys. **67**, 4429 (1990).
[28] D. Smith, V. Parekh, C. E. S. Zhang, W. Donner, T. R. Lee, S. Khizroev, and D. Litvinov, J. Appl. Phys. **103**, 023920 (2008).
[29] S. McVitie and M. Cushley, Ultramicroscopy **106**, 423 (2006).
[30] Y. Togawa, Microscopy **62**, S75 (2013).
[31] X. Yu, D. Morikawa, T. Yokouchi, K. Shibata, N. Kanazawa, F. Kagawa, T. Arima, and Y. Tokura, Nat. Phys. **14**, 832 (2018).
[32] F. V. Lisovskii, E. G. Mansvetova, M. P. Temiryazeva, and A. G. Temiryazev, JETP Lett. **96**, 596 (2013).
[33] S. Miura, M. Mino, and H. Yamazaki, J. Phys. Soc. Jpn. **70**, 2821 (2001).
[34] D. Y. Kim, D. H. Kim, and S. B. Choe, Appl. Phys. Express **9**, 053001 (2016).
[35] F. H. De Leeuw and J. M. Robertson, J. Appl. Phys. **46**, 3182 (1975).